

<https://doi.org/10.1038/s43246-024-00464-w>

# History-dependent nano-photoisomerization by optical near-field in photochromic single crystals

Check for updates

Yuji Arakawa<sup>1</sup>, Kazuharu Uchiyama<sup>1</sup> , Kingo Uchida<sup>2</sup>, Makoto Naruse<sup>3</sup> & Hirokazu Hori<sup>1</sup>

The history dependence of physical systems is promising for solving complex problems. To exploit spontaneous nanometre-scale optical memory for computation, the history dependence must be elucidated. Here, we demonstrate history-dependent or dynamic nano-photoisomerization through the sequential formation of multiple memory pathways in photochromic crystals via optical near-field interactions. Incident photons passing through photoisomerization memory pathways are observed using a double-probe optical near-field microscope, with one probe located on the front surface for local excitation and the other on the rear surface for near-field observations. By performing localised near-field excitation twice but at spatially different positions, negatively correlated near-field output patterns are observed between the first and second memory pathways. We also confirm that the first memory pathway is preserved after the formation of the second memory pathway. This result indicates that photoisomerization using an optical near field in diarylethene crystals has a history dependence, leading to brain-like dynamic information memorisation.

In recent years, computing based on the von Neumann architecture has experienced fundamental difficulties in solving complex problems<sup>1</sup>. Physical and spontaneous processes have the potential to be utilised in intelligent devices and systems beyond conventional architectures<sup>2,3</sup>. Currently, such emerging system architectures are being intensively studied, including neuromorphic computing<sup>4,5</sup>, nature-inspired annealing<sup>6,7</sup>, and photonic decision-making<sup>8</sup>. In general, these principles utilising physical processes for computing are included under the concept of natural intelligence, which relates or associates complex phenomena or structures in natural systems with the problems under study. For example, in the literature, natural computations with amoebas<sup>9</sup> and decision-making with single photons<sup>10</sup> have been demonstrated to solve complex problems using parallelism and history-dependent selection of alternatives by exploiting the non-triviality of physical systems. These studies indicated that the parallelism and history dependence of physical systems are promising resources for solving complex problems.

Functional computation in a physical system requires spontaneous memory structures to be embedded in the physical system. However, the persistent storage of information in the form of light is known to be extremely technologically difficult<sup>11,12</sup> in addition to the difficulty in overcoming the diffraction limit of light for high-density storage<sup>13</sup>. Therefore, in

this study, we focused on the crystal structure of photochromic molecules that memorise light irradiation events in the form of isomerization states at the subwavelength scale via near-field optics. In other words, we utilised the unique intrinsic attributes of photochromic materials<sup>14</sup> and optical near-field interactions at the subwavelength scale<sup>15,16</sup> to overcome the diffraction limit of light.

Nakagomi et al. succeeded in generating subwavelength-scale autonomously formed complex structures in a photochromic material via localised near-field light excitation<sup>17,18</sup>. In their approach, the interplay between the anisotropic deformation of photochromic molecules and localised near-field light yields a chain of transparent regions in the material, hereafter referred to as the ‘memory pathway’. Furthermore, Uchiyama et al. generated Schubert polynomials, which are the foundation of combinatorial mathematics, based on photon statistics observed in complex nanostructures formed in a photochromic material<sup>19</sup>.

However, the unique capability of reconfigurable information storage in the form of photoisomerization at the subwavelength scale has not yet been fully utilised. In other words, it is necessary to examine the addition and erasure of information at the nanometre scale, hereafter referred to as ‘history-dependent nano-photoisomerization’, which is also reflected in the title of this article. As mentioned above, history

<sup>1</sup>University of Yamanashi, 4-3-11 Takeda, Kofu, Yamanashi 400-8511, Japan. <sup>2</sup>Ryukoku University, 1-5 Yokotani, Oe-cho, Seta, Otsu, Shiga 520-2194, Japan.

<sup>3</sup>Department of Information Physics and Computing, Graduate School of Information Science and Technology, The University of Tokyo, 7-3-1 Bunkyo-ku, Tokyo 113-8656, Japan. e-mail: [kuchiyama@yamanashi.ac.jp](mailto:kuchiyama@yamanashi.ac.jp)

dependence is of critical importance for solving complex problems, as observed in neuromorphic computing<sup>4,5</sup>, multi-armed bandit problems<sup>8</sup>, and reinforcement learning<sup>20</sup>.

In the present study, we experimentally demonstrated the sequential formation of multiple memory pathways in photochromic crystals using a double-probe optical near-field microscope. In this microscope, one probe was located on the front side of the photochromic single crystal for local excitation and the other probe was placed on the rear side for observation. By performing localised near-field excitation at the front side, photoisomerization was introduced at the subwavelength scale, leading to the formation of a memory pathway, which was observed by scanning an optical fibre probe located on the rear side.

We examined the history-dependent nano-photoisomerization by changing the spatial position of the front-side local photoexcitation. Specifically, the local optical excitation was repeated twice, denoted as first and second excitations, while the spatial position of the excitation was changed. As demonstrated later, a negative correlation was observed between the optical near-field measurements on the surface of the photochromic material triggered by the first and second excitations. In other words, near-field optical observations from the added memory pathway were mutually exclusive to those from the previously formed original memory pathway. We also confirmed that the first memory pathway was preserved after the addition of the second memory pathway. This result indicates that photoisomerization induced by an optical near field in diarylethene crystals has a history dependence, leading to a dynamic paradigm of computations using light-matter interactions.

## Results and discussion

### Formation and observation of photoisomerization pathways

The photochromic molecule used in this study was diarylethene, which is shown in Figure 1a<sup>21</sup>. It consists of open-ring (**1o**) and closed-ring (**1c**) isomer states and can be isomerised between these states through light irradiation. The open-ring isomer is transparent to visible light and isomerised to the closed-ring isomer under ultraviolet (UV) irradiation (Figs. 1a, b). The closed-ring isomer is opaque and blue in colour and returns to the open-ring isomer state upon photoisomerization with visible light.

The diarylethene molecule exhibits reversible photoisomerization even in the crystalline state, and both isomers are thermally stable<sup>14</sup>.

We obtained a plate-like crystal through recrystallisation using hexane as the solvent and coated the front and rear surfaces of the crystal with a 10-nm-thick Pt layer via sputter deposition for observation using scanning tunnelling microscopy (STM). Figure 1c, d shows the surface height profiles of the prepared samples observed using STM. The surface consisted of a flat surface in the order of molecular length and a step structure of several nanometres in size. The surface structure was stable against photoisomerization, and the topography allowed the comparison of multiple scanning near-field optical microscopic (SNOM) images for positional identification. Furthermore, the flat surface extended over several hundred nanometres, making the sample surface suitable for local excitations and measurements on the spatial scale of approximately 100 nm. See the *Methods* section for further details regarding the crystal samples.

We measured the optical input-output relationship through the photochromic diarylethene single crystal using a double-probe SNOM (Fig. 2a)<sup>17</sup>. One probe was an Au-coated tungsten probe for local excitation and was used to approach the front surface of the crystal, and the other was an optical fibre probe for the local measurement of the optical near-field and was used to approach the rear surface of the crystal, as schematically shown in Fig. 2a. The optical fibre probe on the rear side was scanned for a two-dimensional measurement of the optical near field to measure the input-output relations through the transparent nanostructure within the photochromic material, which is called the memory pathway. Figure 2b, c shows the scanning electron microscopic images of the Au-coated metal and optical fibre probes, respectively. The relative transversal position difference between the tips of the two probes was adjusted within the measurement area (2  $\mu\text{m}$ ) using an established method<sup>17</sup>. The relative misalignment of the two probes was estimated to be less than 1.5  $\mu\text{m}$ . The positional relationship between the two probes was fixed using the high positional accuracy of the STM as the origin of their relative positions in the horizontal plane while performing the measurements mentioned below. See the *Methods* section for further details regarding the probe preparation and alignment method.

The single crystal was initially coloured through irradiation with a UV laser (Vortran Laser Technology, Stradus 375-60; wavelength: 375 nm;

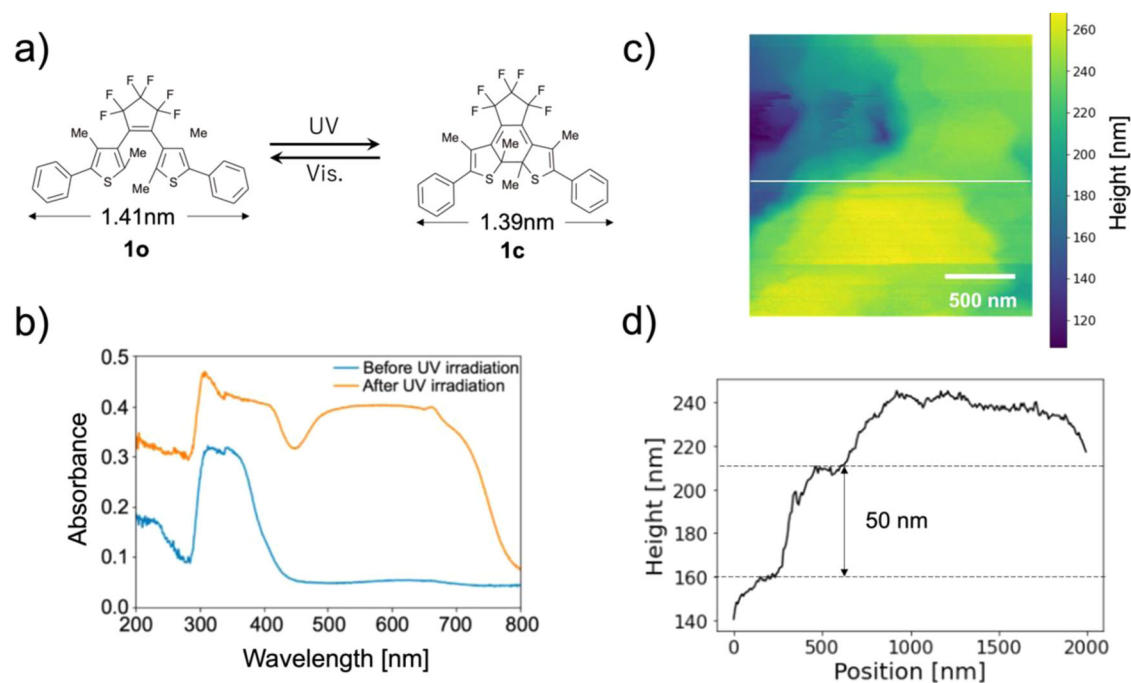


**Fig. 1 | Optical properties and surface structure of the photoisomeric diarylethene crystal.** **a** Photochromic diarylethene molecules and photoisomerizations, **b** absorbance spectra for the transparent and coloured photochromic crystals, **c** STM

topography on the sample surface, **d** height profile along the white line depicted in **c**. STM scanning tunnelling microscopy.

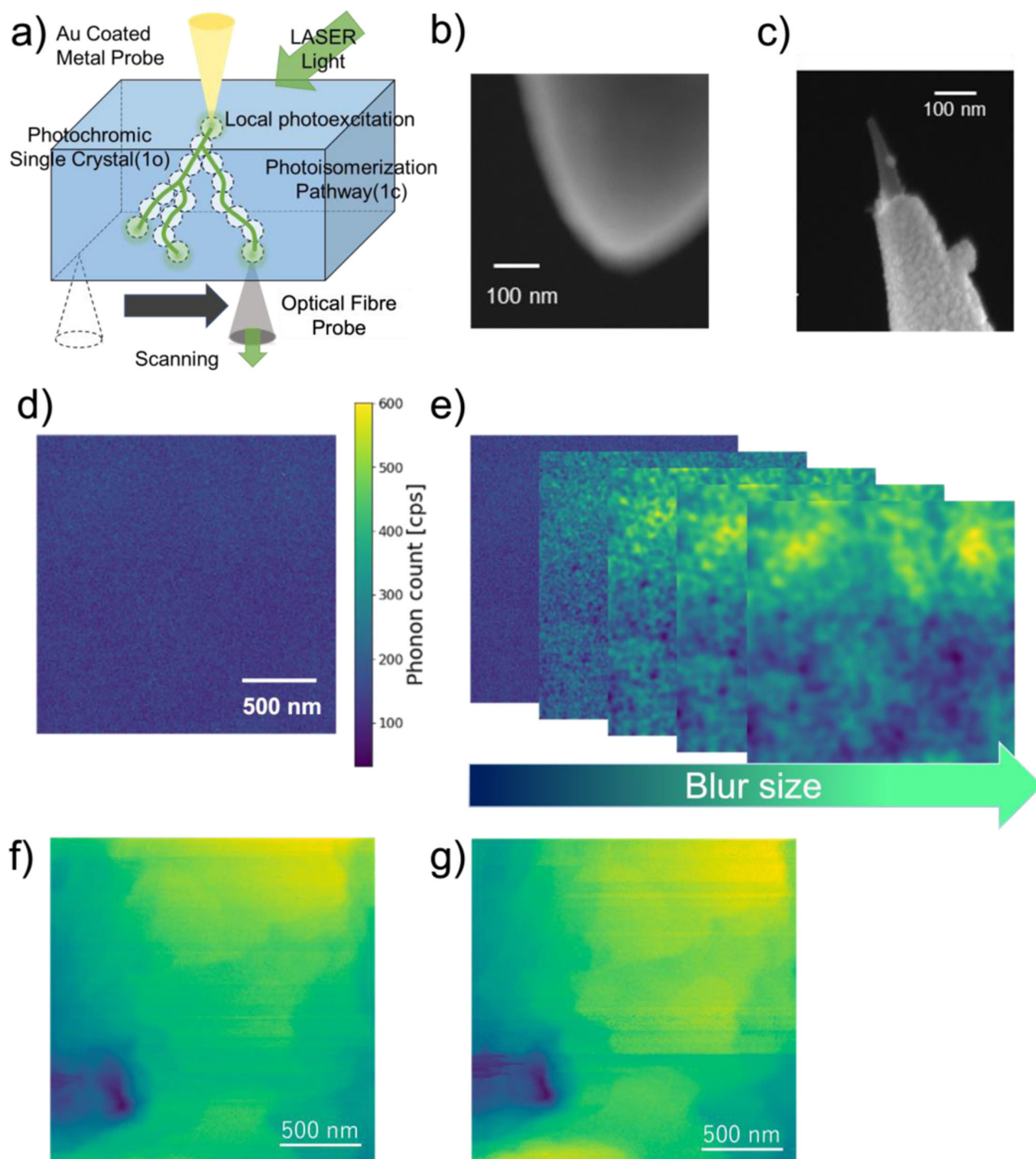


**Fig. 2 | Local excitation and photon detection on a photochromic single crystal.** **a** Schematic diagram of the experiment. Local excitation by the metal probe generates photoisomerization pathways in the crystal, and the photons travelling through the pathway are detected using the optical fibre probe on the rear side, **b** metal probe for local photoexcitation used in the experiment, **c** optical fibre probe

for the local measurement of the optical near field, **d** one of the obtained SNOM images as the output of photoisomerized pathways formed with the chain of anisotropic photoisomerizations, **e** visualisation of the local optical structure with a blur filter of the corresponding scale, **f** first of two sequentially measured topographic images, **g** second image. SNOM scanning near-field optical microscopy.

power:  $\sim 100$  mW/cm<sup>2</sup>) for 30 min. UV irradiation at this wavelength sufficiently coloured the entire sample blue<sup>22</sup>. After moving the two probes 1 nm closer to the sample surface by utilising the capability of the STM apparatus, we irradiated the sample surface with visible laser light (Melles Griot, 85-CGA-020; wavelength: 532 nm; power on the sample surface:  $>100$   $\mu$ W/cm<sup>2</sup>). With the excitation probe fixed, we measured the optical near-field and topography maps on the rear surface of the sample simultaneously. These maps were measured line-by-line in both forward and

reverse scanning directions, making it possible to distinguish between photon detection through the transparent nanostructures and background noise. Based on the acquired topography maps, positional deviations between consecutively measured SNOM data were calculated and used for positional correction when comparing the SNOM data. The measurement time for each image pair was approximately 6 h. The scanning area was 2000-nm<sup>2</sup>, and the resolution was 256  $\times$  256 pixels; hence, the image resolution was 7.8 nm/pixel.

Here, we discuss local optical excitation in this system and the formation of nano-transparent pathways in the crystal<sup>17,18</sup>. The visible light incident on the sample surface was locally enhanced near the probe tip in a subwavelength region approximately the same size as the tip radius, which was approximately 100 nm (Fig. 2b). The enhanced local optical near-field excited and isomerised the photochromic molecules from the closed-ring isomer state to the decolourised transparent opening isomer state. An optical near field has a high spatial frequency, corresponding to a high momentum such that molecules within the local excitation area are isomerised into the transparent state as a cluster from the initially coloured state. The generated transparent cluster has a spatial scale of several tens of nanometres<sup>18,19</sup> and functions as an extended optical near-field source.

Notably, local photoisomerization did not extend to the neighbouring area in an isotropic manner because the crystalline distortion induced by photoisomerization is anisotropic and acts on a spatial scale that is presumably comparable to the optical near field. The destination of the next photoisomerization branches out into multiple options. When one of the options is selected, photoisomerization generates another mechanical distortion that constrains subsequent photoisomerizations. In this manner, a chain of local photoisomerizations in the composite of the optical near field and mechanical distortion field spontaneously generated transparent photoisomerized pathways, as schematically depicted in Fig. 2a. An SNOM image obtained by injecting photons from the same excitation point into the formed nano-photoisomerization pathway is shown in Fig. 2d. However, the raw SNOM image does not show the optical near-field structure well owing to the large dispersion of the number of photons measured at each point. Thus, by applying appropriate blur filters above the spatial resolution of the SNOM probe, the input–output correlation at different scales in the pathway was visualised (Fig. 2e).

It should be emphasised that the pathways were caused by the photoexcitation generated from a single photoexcitation point fixed on the front surface. However, complex subwavelength structures were observed via optical near-field measurements from the rear surface. Based on these findings, we observed that the optical output from an exit point via complex photoisomerization pathways, referred to as ‘memory pathways’, in the nanostructure is complex but inherits individuality.

We had to compare the results of several consecutive scanning near-field optical microscopic measurements, where each measurement time was approximately 6 h. If the amount of thermal drift within that time was greater than the size of the local photoisomerization (approximately 100 nm), the data could not be considered to originate from the same point of continuous local photoexcitation. Figure 2f–g shows the topographic images of two consecutive measurements performed over a period of 6 h using the experimental setup. The shift that maximised the agreement between the two images was estimated to be 2 pixels (approximately 16 nm) in the horizontal direction and 9 pixels (approximately 72 nm) in the vertical direction. The estimated drift rate was approximately 12 nm/h. The drift of the measurement area was smaller than the local optical excitation size for a typical measurement time, which confirms the claim made in this study.

### History-dependent nano-photoisomerization as memory pathways

Figure 3a shows the experimental procedure used to investigate the history dependence in the sequential formation of multiple memory pathways. In step (i), the first memory pathway was formed by local photoexcitation in the initially coloured crystal (Fig. 3a(i)). This is referred to as the first memory pathway (**P1**), and the measured optical near-field map is referred to as **MP1**. In step (ii), we shifted the local excitation point by 1  $\mu\text{m}$  for the formation of the second memory pathway (**P2**) and measured the optical near-field map, referred to as **MP2** (Fig. 3a(ii)). In step (iii), the local excitation point was returned to the optical input point **P1**. We denoted the remeasured memory pathway as **P1'** and the optical near-field map as **MP1'** (Fig. 3a(iii)).

Figure 3b(i)–(iii) shows the three optical near-field images obtained in the same area, **MP1**, **MP2**, **MP1'**, respectively. The distribution of the exit positions of the memory pathway was observed as subwavelength-scale bright spots in optical near-field images. The average number of photons detected per pixel was 22, with a maximum of 198 counts/pixel and a minimum of 3 counts/pixel. The dark count was 4.5 counts/pixel. To eliminate the noise and compensate for small changes in the experimental conditions, we normalised each line of the obtained image by the mean photon count and subsequently blurred the normalised image with a Gaussian filter of 3 pixels, corresponding to approximately 23 nm, which was the measurement resolution of the apparatus. Each image was  $256 \times 256$  pixels for a  $2\text{-}\mu\text{m}^2$  region. Based on the topographic images captured simultaneously, we searched for common areas in the three images. As mentioned above, the thermal drift that caused the relative positions of the probe and sample to shift was approximately 10 nm/h in this experimental setup. The STM image confirmed that the displacement within the measurement time was less than 100 nm, that is, less than the size of the local excitation and measurement. See the *Methods* section for further details.

As shown in Fig. 3c, we extracted nanostructures of approximately 60 nm from the SNOM images via bandpass filtering at a spatial scale of 50–70 nm. Here, we focused on a  $250\text{-nm}^2$  region indicated by the black square in each image in Fig. 3b, to investigate the relationship between the three SNOM images concerning the nanostructures. The solid black circles depict the bright nanostructures observed in **MP1**, and the solid red circles indicate those observed in **MP2**. In **MP1** (Fig. 3c(i)), the bright spots in **MP2** were dark, as indicated by the dashed red circles. By contrast, in **MP2** (Fig. 3c(ii)), the spots which were bright in **MP1** were dark, as indicated by the dashed black circles. In **MP1'** (Fig. 3c(iii)), the spots which were bright in **MP1** were also bright, whereas those which were bright in **MP2** were dark. A comparison of the three SNOM images indicated that additional memory pathways induced by the second local excitation were formed while avoiding the memory pathways previously formed by the first local excitation.

We extracted structures with a spatial bandwidth of 10 nm at various scales (see the *Methods* section for further details regarding the bandpass filter) and evaluated the correlations between the three images. The cross-correlations between **MP1** and **MP2**, **MP1'** and **MP2**, and **MP1** and **MP1'** are shown in Fig. 4a–c, respectively. The higher the correlation coefficient on the vertical axis, the more the photons travelled through the same memory pathway; this is used to evaluate the degree of coincidence of multiple experienced memory pathways. The horizontal axis represents the sizes of the nano-optical structures extracted from the SNOM images using the bandpass filter.

A comparison of **MP1** and **MP2** shown in Fig. 4a shows negative correlations in the optical near-field regime, less than one-quarter of the wavelength ( $\sim 100$  nm), indicating that the nanometre-scale memory paths were different for different local optical excitation points. In other words, the mechanical distortion field generated by the formation of the first memory pathway (**P1**) via photoisomerization exclusively constrained the formation of the second memory pathway (**P2**), leading to the formation of different paths. The comparison between **MP1'** and **MP2** shown in Fig. 4b also exhibited negative correlations; however, their extents were relatively weak compared with those shown in Fig. 4a. This indicates that some of the photons from excitation point **P1'** flowed into the newly formed **P2**. In other words, the memories of **P1** and **P2** generated a mixed memory.

Finally, we compared **MP1** and **MP1'**, which were related to the local optical excitations given at the same point, but before and after adding another memory via **P2** (Fig. 4c). These structures were positively correlated; hence, they were consistent for the same local optical excitation even after adding other memories via **P2**. This consistency indicates the conservation of memory pathways.

Photoisomerization memory pathways are formed in equilibrium between the optical near field and the mechanical distortion field. A new

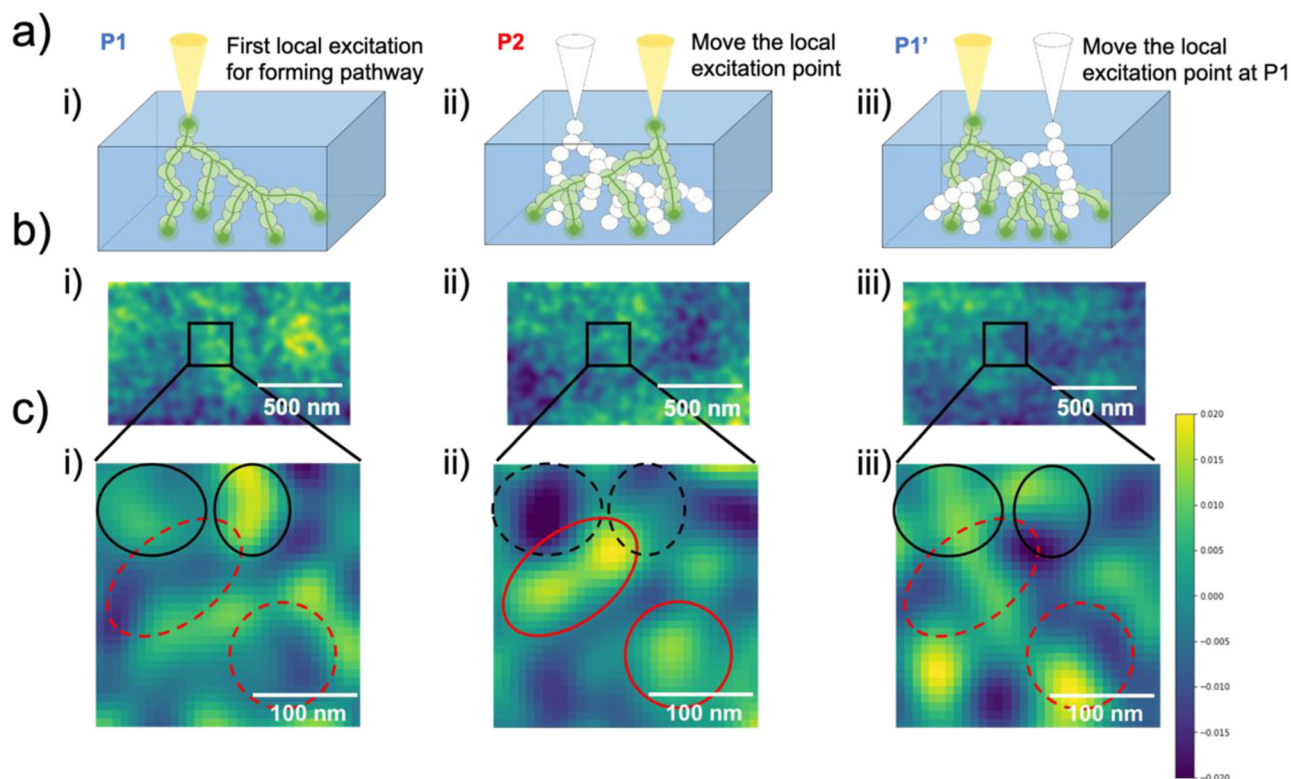


**Fig. 3 | Measurements of multiple memories.** **a** Measurement procedure for history dependence, **b** SNOM images for the three measurements in the same area, **c** magnified SNOM images of the 250-nm<sup>2</sup> area indicated by the black boxes in **b**. SNOM scanning near-field optical microscopy.

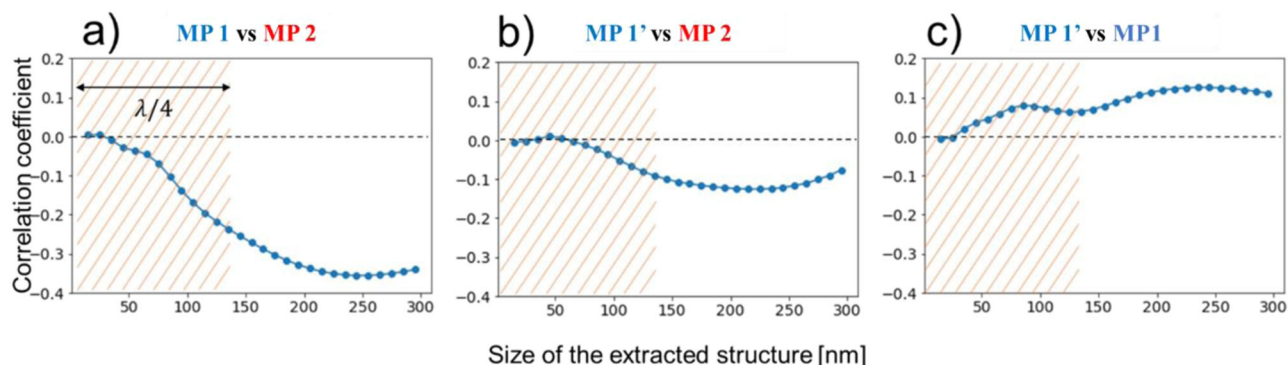


**Fig. 4 | Cross-correlations between the three memory pathways.** Cross-correlations between **a** MP1 and MP2, **b** MP1' and MP2, and **c** MP1 and MP1'.

memory was added under a mechanical distortion field around the existing memory (Fig. 5a). In nanophotocromism in photochromic crystals, a mechanical distortion field generated by the memory produces a probability distribution of photoisomerization as the environment for subsequent memories on the nanometre scale. The new memory pathways tended to pass through the gaps in the existing structures such that the photoexcitation chain along the photoisomerized regions remained independent to avoid the mixing of the optical near-field interaction networks (Fig. 5b).

Here, we provide additional remarks regarding the experiments conducted in this study. After completing the first memory examination at **P1**, the sample was irradiated with UV light for 90 min to completely reset the material before starting the second memory examination at **P2**. Furthermore, we added local photoexcitations at other points and performed SNOM measurements four times in addition to the three SNOM measurements mentioned above (**MP1**, **MP2**, and **MP1'**). First, we could not find apparent nanostructures in the optical near-field maps for other photoexcitations. We speculate that the local excitation point was not fixed sufficiently during the optical near-field measurements; hence, the

memory pathways were not sufficiently formed to be observed on the rear side. In the case of the three photoexcitations (**P1**, **P2**, and **P1'**), we considered that the local excitation probe was well fixed at the same point such that the pathways from the front side to the rear side were sufficiently formed via photoisomerization and observed as optical near fields on the rear side.

The second remark concerns the observation that **MP1** and **MP1'** exhibited a positive correlation although a 90-min recolouring process with UV irradiation was conducted between the observations of **MP1** and **MP1'**. In other words, the original memory pathway was not completely eliminated. This indicates that the memory pathway formed at the nanometre scale via local excitation was resistant to or robust against far-field light irradiation. This resistance may be attributed to the mechanical distortion field around the memory pathway. Similar to the process of pathway formation, history dependence may be observed in the process of pathway elimination. In other words, the formation of local strain fields that are sensitive to the detailed order of elimination may form and determine where the next elimination occurs; as a result, even when all pathways have been

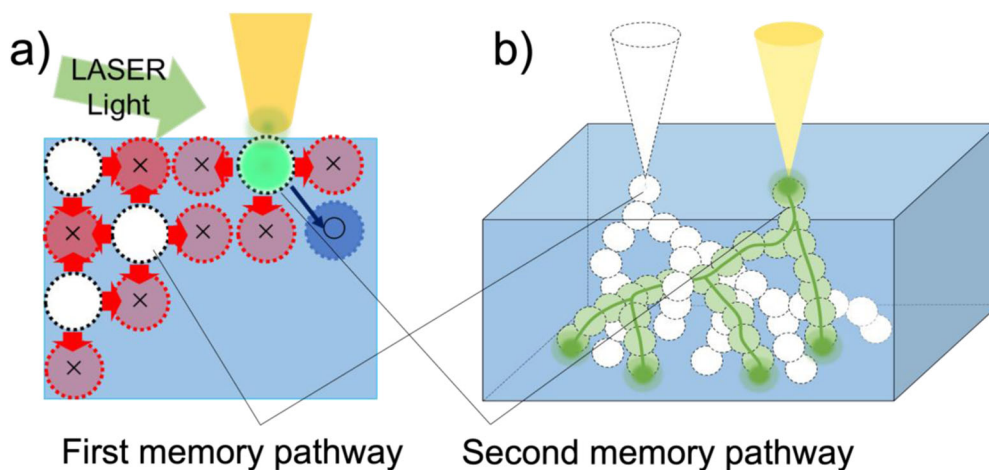


**Fig. 5 | Model of multiple memories in the photochromic crystal.** **a** Two memory pathways formed with history effects. The white circles indicate the first memory. The second memory is formed under the local excitation by the metal tip to avoid the regions forbidden from being photoisomerized, **b** expected relations of the two memories.

eliminated, local distortions may still exist in the orientation of the molecules. In future research, we will investigate whether erasing begins from fine structures or whether memory is retained as a peripheral distortion even after the disappearance of the isomerization path.

The final remark is regarding the mathematical insights into history-dependent nano-isomerization. As mentioned in the Introduction, Uchiyama *et al.* generated a series of ordered structures as matrices deduced from the memory pathways obtained for a fixed single excitation point<sup>19</sup>. The generated series exhibited diversity and appeared almost random; however, they were all correlated because the near-field photon statistics were obtained through fixed-position local excitation<sup>23</sup>. The double memory pathways observed in the present study provided ordered structures, with *two* order structures being correlated. A detailed analysis of this will be conducted in future research. Furthermore, we can explore interesting applications, such as adversarial relationships, which have been intensively studied in the recent research on artificial intelligence<sup>24,25</sup>.

## Conclusion

In this study, we demonstrated the addition of memory pathways and examined the relationship between memories through the optical input–output relationship observed using a double-probe SNOM to investigate the history dependence in the optical near-field-induced formation of photoisomerization memory pathways in a photochromic single crystal. An additional memory pathway was formed exclusively with respect to the original memory pathway. The first memory did not disappear but was partly mixed with the new memory. Such a history-dependent memory was formed spontaneously in the local balance between the optical near field and the mechanical distortion field, which is similar to a memory formed by tuning synaptic connections in the brain. These results indicate the usefulness of diarylethene crystals as dynamic memory structures in non-von Neumann-type devices and systems. In the future, we will further study dynamic and highly multiplexed brain-like memory architectures for intelligent functionalities by exploiting the interplay between photochromism and near-field optics.

## Methods

### Sample preparation

The molecule used in this study was a diarylethene, 1,2-bis(2,4-dimethyl-5-phenyl-3-thienyl)perfluorocyclopentene, whose molecular formula is shown in Fig. 1a. In the open-ring isomer **1o** state, the molecule is transparent to visible light and has a long side of 1.41 nm. In the closed-ring isomer **1c** state, the crystals of **1c** are opaque and blue, with a long side of 1.39 nm. The absorption spectra of the two isomers are shown in Fig. 1b.

Upon irradiation with UV light, the open-ring isomer **1o** isomerizes to the closed-ring isomer **1c**. The closed-ring isomer **1c** is isomerised to the opening isomer **1o** upon irradiation with visible light. The opening and closing of the ring structure at the centre of the molecule changes the conjugation length of the molecule, which in turn changes the absorption spectrum. The symmetry of the crystal structure is the same in the coloured and decoloured states; therefore, photoisomerization proceeds without breaking the crystal lattice.

In this experiment, we used a plate-like single crystal produced via recrystallisation from a hexane solution. The plate thickness was approximately 0.17 mm, and the size of the largest planar surface ((100)-surface) was approximately 0.5 mm. For STM control, the surface was made conductive by coating it with a thin Pt layer of approximately 10 nm in thickness before the initial colouration with UV light. Observation of the sample surface through STM after the initial colouration showed that there were no breaks on the surface of the Pt film and that the surface was flat and suitable for STM scanning (Fig. 1c).

### Probe preparation and alignment method

The tip of the metal probe was sharpened by the electrochemical method to 100 nm using the NaOH solution and coated with a 10-nm-thick gold layer by the sputtering method. The optical fibre tip was sharpened to less than 10 nm via chemical etching with buffered hydrofluoric acid. The tip was coated with a 10-nm-thick Pt layer for position control by STM, and the other part was coated with a 50-nm-thick Pt layer to prevent the detection of propagating light. The final radius of curvature of the tip was approximately 10 nm, which determined the spatial resolution of the optical near-field measurements.

The method for aligning the two probe tips was reported in a previous study<sup>17</sup>. Briefly, the alignment of the two tips was confirmed using the capacitance between the two probes in two dimensions. After alignment, we brought the two probe tips close together and confirmed their relative positions with the resolution of the STM method.

### Determination of the common area in SNOM images

We measured the optical near-field and topographical maps at the same location and time. In scanning probe measurements at room temperature, thermal drift of the relative positions of the sample and tip is inevitable. In this experiment, we confirmed that the drift was smaller than the size of the local photoexcitation (~100 nm) while performing the measurements shown in Fig. 3 based on the STM images. To subtract the drift in the interval of the three measurements, we found a common area in the STM images for comparison with the SNOM images captured in the same area. The

resolution for subtraction was determined from that of the STM image, which was 7.8 nm.

### Extraction of a certain spatial structure from the SNOM images

The SNOM images contained information regarding the optical near-field intensity in the vicinity of the scanning probe and the propagating light distribution that could not be removed. To remove the modulation by incident light (temporal changes in detector sensitivity and laser intensity), we subtracted the mean intensity from each line of the SNOM images. In the SNOM images modified by subtraction (Fig. 3b), large structures with a scale equal to the propagating light wavelength of approximately 500 nm were observed. To investigate the correlation between the SNOM images, we separated the optical near-field components from the propagating light components to extract appropriate scale information from the SNOM images using a bandpass filter. Specifically, when the obtained SNOM image was represented by a two-dimensional matrix  $M$ , we denoted the Gaussian filtered matrix with a standard deviation of  $L$  (nm) by  $M_{G(L)}$ . We used the following equation to extract the structures from  $L_1$  (nm) to  $L_2$  (nm), that is,  $MB(L_1, L_2)$ :

$$MB(L_1, L_2) = \left( M - M_{G(L_2)} \right)_{G(L_1)},$$

assuming  $L_1 < L_2$ . Figure 3c shows  $MB(50\text{nm}, 70\text{nm})$  with a bandwidth of 20 nm. In Fig. 4, the point at 100 nm (twice the centre standard deviation of 50 nm), for example, was calculated using  $MB(45\text{nm}, 55\text{nm})$  with a bandwidth of 10 nm.

### Data availability

The data that support the findings of this study are available upon reasonable request from the authors.

Received: 14 July 2022; Accepted: 23 February 2024;

Published online: 01 March 2024

### References

- Wetzstein, G. et al. Inference in artificial intelligence with deep optics and photonics. *Nature* **588**, 39–47 (2020).
- Inoue, K., Nakajima, K. & Kuniyoshi, Y. Designing spontaneous behavioral switching via chaotic itinerancy. *Sci. Adv.* **6**, eabb3989 (2020).
- Kitayama, K. et al. Novel frontier of photonics for data processing—photonics accelerator. *APL Photonics* **4**, 090901 (2019).
- Marković, D., Mizrahi, A., Querlioz, D. & Grollier, J. Physics for neuromorphic computing. *Nat. Rev. Phys.* **2**, 499–510 (2020).
- Shastri, B. J. et al. Photonics for artificial intelligence and neuromorphic computing. *Nat. Photonics* **15**, 102–114 (2021).
- Yamaoka, M. et al. 20k-spin Ising chip to solve combinatorial optimization problems with CMOS annealing. *IEEE J. Solid St. Circuits* **51**, 303–309 (2015).
- Honjo, T. et al. 100,000-spin coherent Ising machine. *Sci. Adv.* **7**, eabh0952 (2021).
- Naruse, M. et al. Decision making photonics: solving bandit problems using photons. *IEEE J. Sel. Top. Quantum Electron.* **26**, 7700210 (2019).
- Aono, M. et al. Amoeba-inspired nanoarchitectonic computing: solving intractable computational problems using nanoscale photoexcitation transfer dynamics. *Langmuir* **29**, 7557–7564 (2015).
- Naruse, M. et al. Single-photon decision maker. *Sci. Rep.* **5**, 13253 (2015).
- Langenhorst, R. et al. Fiber loop optical buffer. *J. Lightwave Technol.* **14**, 324–335 (1996).
- Krauss, T. F. Slow light in photonic crystal waveguides. *J. Phy. D: Appl. Phys.* **40**, 2666 (2007).

- van de Nes, A. S., Braat, J. J. M. & Pereira, S. F. High-density optical data storage. *Rep. Prog. Phys.* **69**, 2323 (2006).
- Irie, M. *Diarylethene Molecular Photoswitches: Concepts and Functionalities* (Wiley-VCH, GmBh, 2021).
- Ohtsu, M. & Hori, H. *Near-field nano-optics: from basic principles to nano-fabrication and nano-photonics* (Springer, 1999).
- Naruse, M., Tate, N., Aono, M. & Ohtsu, M. Information physics fundamentals of nanophotonics. *Rep. Prog. Phys.* **76**, 056401 (2013).
- Nakagomi, R. et al. Nano-optical functionality based on local photoisomerization in photochromic single crystal. *Appl. Phys. A* **124**, 10 (2018).
- Nakagomi, R. et al. Nanometre-scale pattern formation on the surface of a photochromic crystal by optical near-field induced photoisomerization. *Sci. Rep.* **8**, 17474 (2018).
- Uchiyama, K. et al. Generation of Schubert polynomial series via nanometre-scale photoisomerization in photochromic single crystal and double-probe optical near-field measurements. *Sci. Rep.* **10**, 2710 (2020).
- Sutton, R. S. & Barto, A. G. *Reinforcement learning: an introduction* (MIT press, 1998).
- Irie, M., Fukaminato, T., Matsuda, K. & Kobatake, S. Photochromism of diarylethene molecules and crystals: memories, switches, and actuators. *Chem. Rev.* **114**, 12174 (2014).
- Irie, M., Kobatake, S. & Horichi, M. Reversible surface morphology changes of a photochromic diarylethene single crystal by photoisomerization. *Science* **291**, 1769 (2001).
- Uchiyama, K. et al. Order recognition by Schubert polynomials generated by optical near-field statistics via nanometre-scale photochromism. *Sci. Rep.* **12**, 19008 (2022).
- Alqahtani, H., Kavakli-Thorne, M. & Kumar, G. Applications of generative adversarial networks (gans): an updated review. *Arch. Computat. Methods Eng.* **28**, 525–552 (2021).
- Naruse, M. et al. Generative adversarial network based on chaotic time series. *Sci. Rep.* **9**, 12963 (2019).

### Acknowledgements

This work was supported in part by the CREST project (JPMJCR17N2) funded by the Japan Science and Technology Agency and Grants-in-Aid for Scientific Research (JP20H00233, JP21K04925) funded by the Japan Society for the Promotion of Science.

### Author contributions

H.H., K.U.2 and M.N. directed the project. Y.A., K.U.1 and H.H. designed the experimental strategy and methods. K.U.2 prepared the photochromic materials. Y.A. and K.U.1 performed near-field optics experiments. Y.A. and K.U.1 analysed the data. Y.A., K.U.1 and M.N. wrote the paper, and all the authors contributed to the preparation of the manuscript.

### Competing interests

The authors declare no competing interests.

### Additional information

**Correspondence** and requests for materials should be addressed to Kazuharu Uchiyama.

**Peer review information** *Communications Materials* thanks the anonymous reviewers for their contribution to the peer review of this work. Primary Handling Editors: Klaas-Jan Tielrooij and Aldo Isidorio.

**Reprints and permissions information** is available at <http://www.nature.com/reprints>

**Publisher's note** Springer Nature remains neutral with regard to jurisdictional claims in published maps and institutional affiliations.

**Open Access** This article is licensed under a Creative Commons Attribution 4.0 International License, which permits use, sharing, adaptation, distribution and reproduction in any medium or format, as long as you give appropriate credit to the original author(s) and the source, provide a link to the Creative Commons licence, and indicate if changes were made. The images or other third party material in this article are included in the article's Creative Commons licence, unless indicated otherwise in a credit line to the material. If material is not included in the article's Creative Commons licence and your intended use is not permitted by statutory regulation or exceeds the permitted use, you will need to obtain permission directly from the copyright holder. To view a copy of this licence, visit <http://creativecommons.org/licenses/by/4.0/>.

© The Author(s) 2024